Beamline 6.3.2

Calibration and Standards; EUV Optics Testing; Atomic, Molecular, and Materials Science

Angle-dependent soft x-ray emission spectra of hexagonal boron nitride
Muramatsu, Y., R.C.C. Perera

Layer-structure-distribution in the sample plane of Mo/Si multilayers measured by total-electron-yield x-ray standing wave methods
Muramatsu, Y., H. Takenaka, E.M. Gullikson, R.C.C. Perera

Resolving magnetic and chemical correlation lengths in CoPtCr-based recording media
Hellwig, O., D.T. Margulies, B. Lengsfield, E. E. Fullerton, J.B. Kortright

Resonant small angle x-ray scattering of polymers at the C-K edge
Koprinarov, I., G. Mitchell, B. Landes, M. Devon, J. Kortright

Soft x-ray emission and absorption spectra in the Si L region of polysilanes
Muramatsu, Y., M. Fujino, E.M. Gullikson, R.C.C. Perera

Soft x-ray spectroscopy of noble gas atoms doped in solid matrices
Muramatsu, Y., R.C.C. Perera

X-ray absorption studies of the cBN composites with different bonding phases
Benko, E., K. Lawniczak-Jablonska, P. Nachimuthu, I.N. Demchenko, E. Piskorska, P. Klimczyk, R.C.C. Perera, A. Wlochowicz, A. Benko, T.L. Barr

Angle-Dependent Soft X-Ray Emission Spectra of Hexagonal Boron Nitride

Y. Muramatsu[1] and R. C. C. Perera[2]
[1]*Japan Atomic Energy Research Institute, Sayo-gun, Hyogo 679-5148, Japan*
[2]*CXRO, Lawrence Berkeley National Laboratory, Berkeley, California 94720, USA*

Hexagonal boron nitride (*h*-BN) is a basic boron compound, which has been widely used as a reference sample in soft x-ray spectroscopy. It adopts a layered structure similar to graphite. To obtain detailed structural information for *h*-BN using soft x-ray emission spectroscopy, we have measured its angle-dependent soft x-ray emission spectra.

Commercially obtained *h*-BN power pressed on indium sheets and pyrolytic (*p*) BN plate was used for spectroscopic measurements. Soft x-ray emission spectra in the B *K* and N *K* regions were measured using a grating x-ray spectrometer installed in the undulator beamline, BL-8.0.1. The photon energy of the monochromatized incident beam was tuned to about 230 eV (for B *K*) and 430 eV (for N *K*). The incident angle (θ) of the monochromatized beam to the sample surface was adjusted to 15, 45 and 75 degrees. Measured x-ray emission spectra were analyzed using discrete variational (DV)-Xα molecular orbital calculations.

Figure 1 shows the angle-dependent B *K* and N *K* x-ray emission spectra of *p*-BN. In the B *K* spectra, intensity of the high-energy shoulder near 184 eV increases as θ increases. Intensities of the low-energy satellite near 170 eV and the low-energy shoulder near 178 eV both decrease as θ increases. In the N *K* spectra, intensity of the high-energy peak at 398.5 eV drastically increases as θ increases, while intensity of the low-energy shoulders near 385 eV and 390 eV decrease as θ increases. Upper panels of Figure 2 show the calculated density-of-states (DOS) spectra of occupied B2p- and N2p-orbitals in the model cluster of $B_{48}N_{48}H_{24}$. These calculated DOS spectra reproduce the x-ray emission spectra measured with an incident angle of 45 degrees. Lower panels of Figure 2 show the B2p- and N2p-DOS spectra calculated by considering the contributions of σ- and π-components in x-ray emission. In the B2p-DOS spectra, intensity of the high-energy shoulder (near -4 eV) increases as θ increases. Intensities of the low-energy shoulder (-10 eV) and low-energy peak (-18 eV) decrease as θ increases. In the N2p-DOS spectra, intensity of the high-energy peak (-2 eV) increases as θ increases, while intensities of the low-energy shoulders (-6 eV and –10 eV) decrease as θ increases. These calculated spectra well reproduce the measured angle-dependent x-ray emission spectra. Thus, it can be confirmed that angle-dependent x-ray emission measurements will provide detailed structural information on *h*-BN.

We thank Dr. J. Denlinger of the Lawrence Berkeley National Laboratory for his help and support in performing x-ray emission measurements. This work is supported by the Hyogo Science and Technology Association and the US Department of Energy under contract No. DE-AC03-76SF00098.

Principal Investigator: Yasuji Muramatsu, Japan Atomic Energy Research Institute. Email: murama@spring8.or.jp. Telephone: +81-791-58-2601.

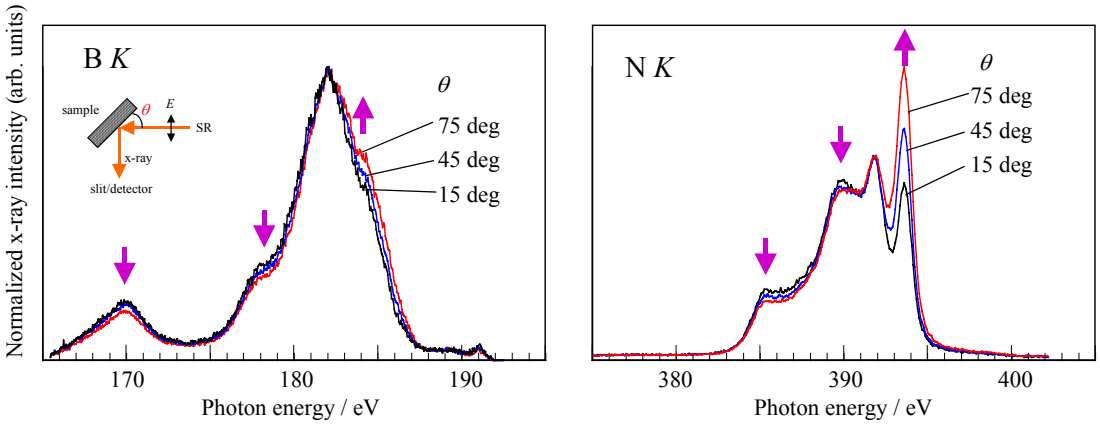

Figure 1 Angle-dependent x-ray emission spectra in the B *K* (left panel) and N *K* (right panel) regions of *p*-BN.

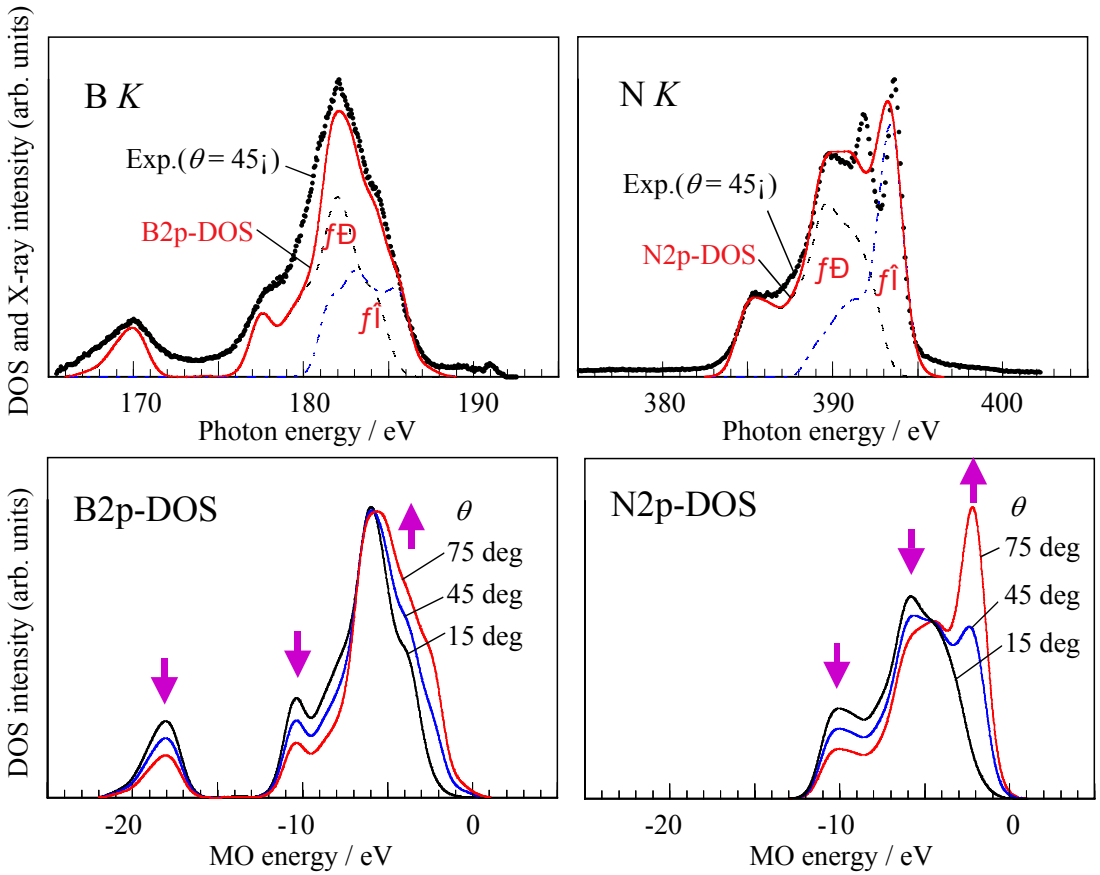

Figure 2 Upper panels show the occupied B2p- and N2p-DOS spectra of the $B_{48}N_{48}H_{24}$ model cluster. X-ray emission spectra measured with an incident angle of 45 degrees are superimposed on the calculated spectra. Lower panels show the angle-dependent B2p- and N2p-DOS spectra with incident angles of 15, 45 and 75 degrees.

Layer-Structure-Distribution in the Sample Plane of Mo/Si Multilayers Measured by Total-Electron-Yield X-Ray Standing Wave Methods

Y. Muramatsu[1], H. Takenaka[2], E. M. Gullikson[3], and R. C. C. Perera[3]

[1]*Japan Atomic Energy Research Institute, Sayo-gun, Hyogo 679-5148, Japan*

[2]*NTT Advanced Technology Corporation, Musashino-shi, Tokyo 180-8585, Japan*

[3]*Center for X-Ray Optics, Lawrence Berkeley National Laboratory, Berkeley, California 94720, USA*

Total-electron-yield (TEY) x-ray standing-wave measurements of multilayer x-ray mirrors have been performed, by monitoring sample photocurrents in BL-6.3.2 to obtain information on their layer/interface structure. Specifically, we have measured mapping spectra of x-ray standing-wave signals in a Mo/Si multilayer at normal incidence, which visibly illustrates the spatial distribution of layer structure in the sample plane.

The Mo/Si multilayer x-ray mirror, deposited on a 4-inch silicon wafer, consists of 50 periods of 19.6-Å Mo and 45.2-Å Si layers. The multilayer x-ray mirror sample is mounted on a sample holder in the reflectometer and a wire is connected to monitor the sample photocurrent. In total electron yield (TEY) x-ray absorption spectral measurements, x-ray standing-wave structure is observed when the photon-energy/wavelength of incident x-rays and the incident angle satisfy the Bragg reflection condition of the multilayer sample.

Figure 1 shows the TEY x-ray standing-wave spectra of a Mo/Si multilayer mirror measured along the 4-inch-wafer-size sample plane at the center (denoted by A in the Figure), middle (Bx, By) and periphery (Cx, Cy) positions. In the center position spectrum, standing-wave structures are observed near 96 eV and the standing-wave peak is observed at 97.68 eV. In the spectra of the middle and periphery positions, standing-wave structures are clearly shifted to higher-energy regions. Figure 2 shows the mapping spectrum of TEY x-ray standing-wave signals over the quarter of the 4-inch-wafer-size Mo/Si multilayer mirror measured with an incident angle of 90°. The photon energy of incident x-rays is fixed at 97.68 eV, identical to the peak energy of the center position x-ray standing-wave. The spot size of incident x-rays on samples is estimated to be less than 0.5 mm^{ϕ}, and spectra are obtained using a 1-mm step scan along the x- and y-axes. This figure depicts periodic-length-changes of Mo/Si layers in the sample plane; the Mo/Si layers gradually become shorter from the center toward the periphery. The contour line also reveals a distribution of layer structure that is slightly wider along the y-axis than along the x-axis. This implies the sputtering source gas used in the deposition process of the multilayers is distributed slightly offset from the y-axis. These results indicate that TEY x-ray standing-wave measurements are useful for evaluating the layer/interface structure of multilayer x-ray mirrors.

We express thanks to Dr. H. Ito and Dr. K. Nagai of the NTT Advanced Technology Corporation for the preparation of multilayer samples. This work is supported by the Hyogo Science and Technology Association and the US Department of Energy under contract No. DE-AC03-76SF00098.

Principal investigator: Yasuji Muramatsu, Japan Atomic Energy Research Institute. Email: murama@spring8.or.jp. Telephone: +81-791-58-2601.

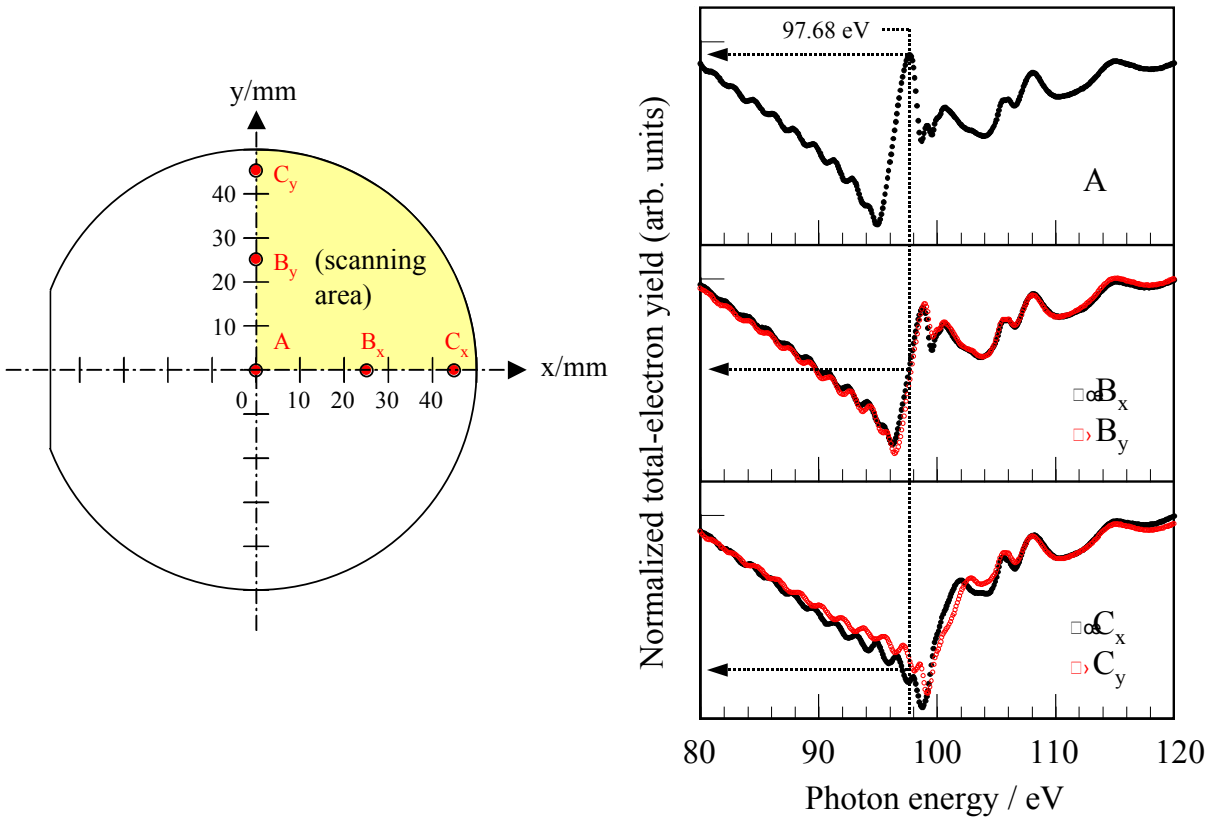

Figure 1 TEY x-ray standing-wave spectra of the Mo/Si multilayer measured at the center (denoted by A), middle (Bx, By), and edge (Cx, Cy) positions along the 4-inch sample plane.

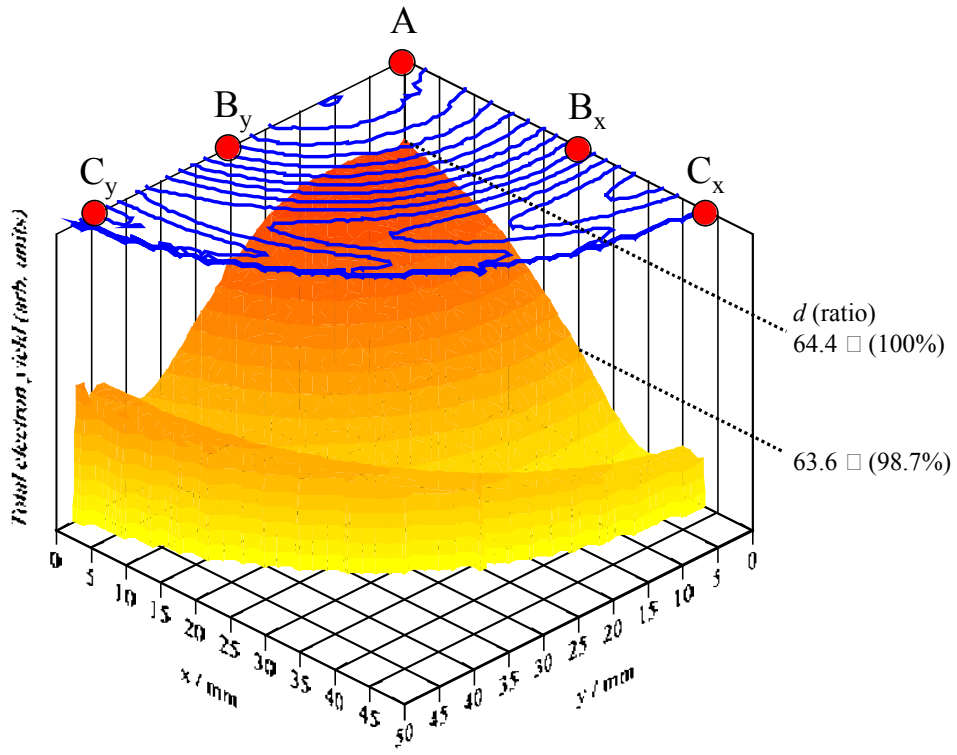

Figure 2 Mapping spectrum of the TEY x-ray standing-wave signals in the quarter of the 4-inch-wafer-size Mo/Si multilayer measured with an incident angle of 90°. The photon energy of incident x-rays is fixed at 97.68 eV.

Resolving magnetic and chemical correlation lengths in CoPtCr-based recording media

O. Hellwig,[1] J. B. Kortright,[2] D. T. Margulies,[1] B. Lengsfield,[1] and E. E. Fullerton[1]
[1]IBM Almaden Research Center, San Jose, California 95120, USA
[2]Materials Sciences Division, Ernest Orlando Lawrence Berkeley National Laboratory, University of California, Berkeley, California 94720, USA

GRANULAR RECORDING MEDIA

Current magnetic recording media consists of chemically segregated, polycrystalline grains whose grain-centers are ferromagnetic with in-plane anisotropy and whose grain boundaries are nominally non-magnetic [1]. This chemically and magnetically heterogeneous microstructure has evolved through several generations of recording media via an increasingly complex set of alloys from CoCr to CoPtCr to CoPtCrB. The additives Cr and later B are known to segregate to and produce nonmagnetic grain boundary phases that were believed to reduce exchange coupling between adjacent grains, thereby enabling sharper bit transitions and higher recording density [2]. Chemical heterogeneity associated with these films is resolved using high-resolution TEM and micro-EELS [3]. It has remained difficult, however, to directly measure the magnetic correlation lengths giving the distance over which grain-to-grain magnetism is correlated.

We have found that both magnetic and chemical heterogeneity in recording media films are strong scattering sources when tuned to specific soft x-ray core resonances to enhance contrast [4,5]. This transmission small-angle scattering (SAS) measurement positions the scattering vector q in the film plane to optimize coupling to in-plane structure (Fig. 1b, inset) [6]. Although soft x-ray wavelengths limit the maximum q, spatial resolution to 1 nm is available.

Q-RESOLVED RESONANT SCATTERING

SAS q scans measured at the resonant intensity peaks at the Co and Cr L_3 lines are shown in Fig. 1. Scans of the common underlayer structure (without any media layer) reveal the contributions from the underlayer and the SiN membrane. These scans are almost featureless, with enhanced low q scattering that is also observed in scattering from the substrate alone, and with a weak, broad peak at $q \cong 0.015$ Å^{-1} observed at the Cr resonance. For the samples with media layers there is additional, strong SAS at both the Cr and Co edges arising from the media layer. This scattering is strongly resonantly enhanced, as is illustrated in Fig. 1b by the 10-fold decrease in scattering just 10 eV below the Co L_3 peak (dashed line) compared to that measured at the peak (open circles). Similarly strong and sharp resonant enhancements are observed near the Cr L_3 line.

The SAS scans from the different media samples show similar features. The Cr-edge data has a peak at $q \cong 0.07$ Å^{-1} for all samples. This peak results from interference between neighboring scattering centers separated by $2\pi/q \cong 100$ Å, typical of grain diameters observed in TEM images of media grown on similar underlayers [2]. We attribute this Cr resonant peak to the average grain diameter of the media. It is well established that chemical segregation during the growth of CoCr alloys involves Cr diffusion to the grain boundaries resulting in a magnetic Co-rich core of the grain with non-magnetic or weakly magnetic Cr-rich grain boundaries [6,7], as shown schematically in Fig. 1b. Thus, by tuning to the Cr edge, we enhance the chemical contrast between the magnetic grain core and the Cr-rich grain boundaries.

The Co-edge scattering is expected to arise from both magnetic and chemical correlations (and their interference). These data show the same interference peak at $q \cong 0.07$Å^{-1} that was observed in the

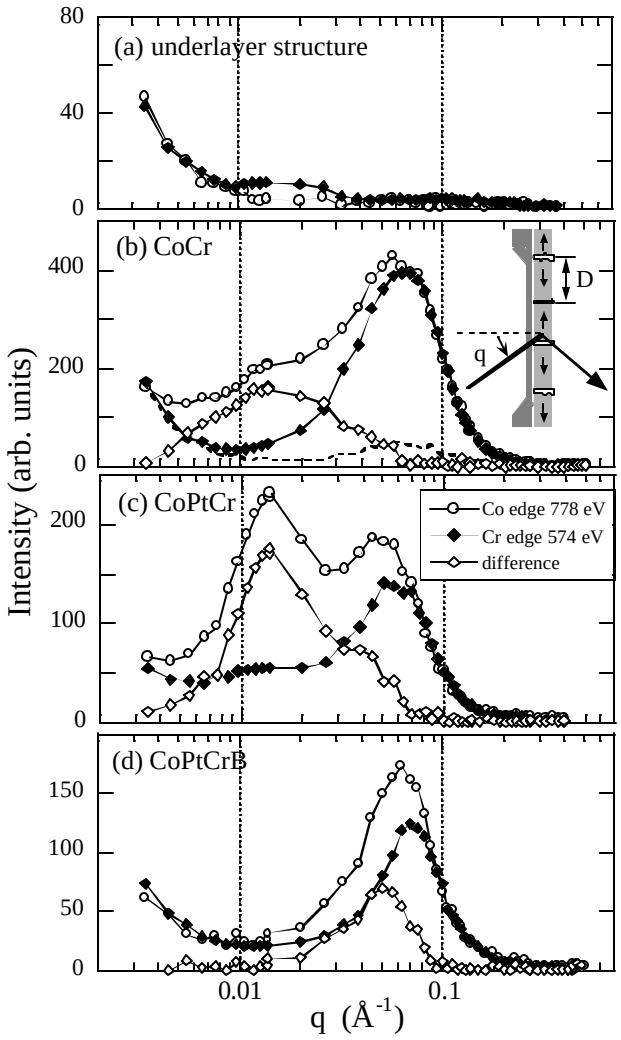

Figure 1. Resonant SAS from the underlayer structure without media layer (a) and from CoCr (b), CoPtCr(c), and CoPtCrB (d) media measured at the Co and Cr L3 lines as indicated. The inset shows the scattering geometry and media layer with magnetic grains (diameter D) with the in-plane magnetization direction represented by the arrows and nonmagnetic grain boundaries. The open diamonds are the difference between the Co- and Cr-edge data. The dashed line in (b) is the nonresonant scattering measured 10 eV below the Co edge.

Cr-edge data, as well as additional scattering at significantly lower q values. The observation of high-q resonant scattering from the grain structure at both the Co and Cr edges confirms that this scattering arises from in-plane compositional variations of Co and Cr. The additional lower-q scattering arises predominantly from correlated magnetic regions larger than the grain size. For the CoPtCr film (Fig. 1c), this additional scattering is clearly resolved as a peak at $q \cong 0.015$ Å^{-1} corresponding to a real space distance of ≅ 400 Å. The difference of the Co and Cr resonant scans (scaled to match at high q) results from Co magnetic-magnetic correlations and magnetic-charge interference, with the former dominating the low-q peak and the latter contributing progressively to increasing q. The low-q peak is thus a measure of the magnetic correlation length in these media films.

Boron additions are seen to reduce the magnetic correlation length from 4-5 times the chemical grain size to closely approach the grain size, consistent with improved recording performance and inferred magnetic correlation lengths from recording signal to noise measurements.

MODELING ENERGY SPECTRA

The above interpretation of magnetic and chemical peaks is qualitative. One approach to independent, quantitative determination of the scattering sources contributing to the peaks is to model the energy spectra of the scattering at each peak [5]. Measured Co L_3 energy spectra at these two peaks for the CoPtCr sample are shown as symbols in Fig. 2, and clearly have very different shape. Modeling these resonant shapes requires measured values of charge and magnetic atomic scattering factors f for Co. These were obtained from transmission absorption measurements of the saturated media film with linear and circular polarization, followed by Kramers-Kronig transformation of the imaginary part of these quantities to obtain their real parts. Non-resonant f values for Cr and Pt were taken from tabulated values [9].

Following standard SAS formalisms, the amplitude for different scattering sources is given by the difference of amplitudes of the two phases defining the heterogeneity. The simplest model for pure magnetic scattering yields amplitude proportional to the magnetic part of f for Co [5, 6]. The corresponding intensity is scaled and plotted in Fig. 2, with a small non-resonant background added.

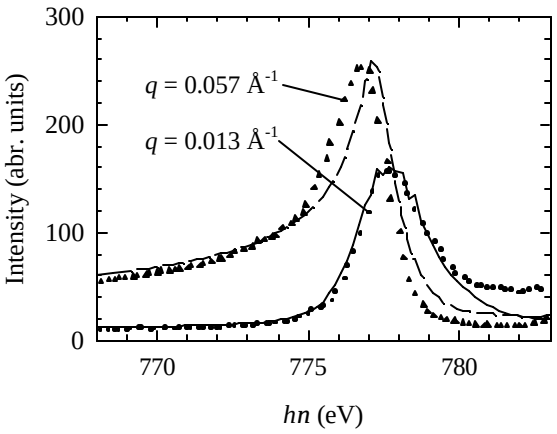

Figure 2. SAS energy spectra across the Co L_3 line of the CoPtCr media at the high- and low-q peaks (symbols). Model spectra based on measured Co resonant scattering factors (lines) confirm the magnetic and chemical origin of the two peaks.

The good agreement of model and measured spectra confirms the magnetic origin of the low-q peak and thus that magnetic correlation lengths in this sample are several times the chemical grain size. Modeling the high-q spectrum requires postulating compositions of the segregated phases at the grain boundaries and centers, forming the appropriate scattering amplitudes of these two phases as linear combinations of elemental scattering factors, and squaring the difference of these amplitudes to obtain the intensity spectrum. A model spectrum is scaled and plotted with the high-q data in Fig. 2, confirming that the high-q peak is consistently modeled assuming chemical origin. Details showing that this model is sensitive to the composition of segregated phases are in ref. [5].

CONCLUSIONS

Resonant SAS contrast at Co and Cr $L_{2,3}$ lines strongly enhances both magnetic and chemical scattering in recording media films. Since Co and Cr enhancements have different sensitivity to chemical and magnetic heterogeneity, their relative behavior allows clear separation of chemical and magnetic length scales and a very direct measurement of magnetic correlation lengths in granular recording media. The addition of B to the media alloys significantly reduces the magnetic correlation lengths [4]. Modeling of resonant energy spectra at the Co L_3 edge using measured resonant Co scattering factors quantitatively confirms magnetic and chemical scattering sources and provides an estimate of the composition of segregated phases yielding the chemical scattering [5].

REFERENCES

1. H. N. Bertram, Theory of Magnetic Recording (Cambridge University Press, Cambridge, U.K.) 1994.
2. M. Doerner, *et al*., IEEE Trans. Magn. 37 (2001) 1052.
3. M. Doerner, *et al*., IEEE Trans. Magn. 36 (2000) 43.
4. O. Hellwig, D. T. Marguiles, B. Lengsfield, E. E. Fullerton, J. B. Kortright, Appl. Phys. Lett. 80 (2002) 1234.
5. J. B. Kortright, O. Hellwig, D. T. Marguiles, E. E. Fullerton, J. Magn. and Magn. Mater. 240 (2002) 325.
6. J. B. Kortright, *et al.*, Phys. Rev. B 64 (2001) 092401.
7. J. E. Wittig, *et al*., IEEE Trans. Magn. 34 (1998) 1564.
8. N. Inaba, Y. Uesaka, and M. Futamoto, IEEE Trans. Magn. 36 (2000) 54.
9. B. L. Henke, E. M. Gullikson, J. C. Davis, At. Data Nucl. Data Tables 54 (1993) 181; and at http:/www-cxro.lbl.gov/optical_constants/.

This work and JBK were supported by the Director, Office of Energy Research, Office of Basic Energy Sciences, Materials Science Division, of the U.S. Department of Energy under Contract No. DE-AC03-76SF00098.

Principal investigator: Eric Fullerton, IBM Almaden Research Center. Email: eef@almaden.ibm.com. Telephone: (408) 927-2430.

Resonant Small Angle X-Ray Scattering of Polymers at the C-K edge

Ivaylo Koprinarov[1], Gary Mitchell[2], Brian Landes[2], Mike Devon[3] and Jeff Kortright[4]
[1]BIMR, McMaster University, Hamilton, ON, Canada L8S 4M1
[2]Analytical Sciences, The Dow Chemical Company, 1897 Building, Midland, MI, 48667
[3]Emulsion Polymers Research, The Dow Chemical Company, 1604 Building, Midland, MI 48667
[4]Lawrence Berkeley National Lab, Berkeley, CA 94720

INTRODUCTION

Small-angle x-ray scattering is a very valuable technique which complements microscopic techniques by providing statistically averaged information on polymer morphology. For the hard x-rays, scattering intensity is determined by the electron density contrast between two phases [1]. There are situations where this contrast mechanism is not sufficient, e.g. the case where the material has more than two phases or the electron density contrast is not sufficient to give detectable scattering.

We have begun a program to use resonant scattering energies to enhance the information content and signal to noise ratios in small angle x-ray scattering of polymers. Resonant x-ray scattering is a well known phenomenon and has been demonstrated for hard x-ray energies [2], but to our knowledge has never been attempted at the C1s edge, although it has been applied to study magnetic materials [3]. The soft x-ray energy places fairly formidable restrictions on sample preparation conditions. We have performed proof of principle experiments using latex polymers made from polystyrene and polymethylmethacrylate. The early results are very exciting and indicate that this technique may have several interesting and useful applications in the field of polymer characterization.

The x-ray scattering amplitude (f) is a function of energy and is a complex number and the imaginary part (f_2) is due to absorption [4]:

$$f(E) = f_1(E) + i f_2(E) \quad (1)$$

$$f_2(E) = \frac{\sigma_a(E)}{2 r_e \lambda} \quad (2)$$

$$f_1(E) = Z + \frac{1}{\pi r_e hc} \int_0^{\infty} \frac{\varepsilon^2 - \sigma_a(\varepsilon)}{E^2 - \varepsilon^2} \, d\varepsilon \quad (3)$$

The Kramer's Kronig dispersion relation relates the real and imaginary parts, where σ_a is the absorption cross section, λ is the wavelength, r_e is the classical electron radius, h is Planck's constant, c is the speed of light and Z is the atomic number.

Well away from an absorption resonance ($\sigma_a \Rightarrow 0$), x-ray scattering intensity (f^2) is determined by the electron density contrast between the (difference in Z) phases, as mentioned above. Near resonance, however, the intensity is modulated by the absorption cross section. Thus we can make use of the very same near edge x-ray absorption spectral features that have proven useful in x-ray microscopy [5], so-called *near-edge x-ray absorption fine structure* (NEXAFS) [6], to provide chemical contrast between different phases in a polymer system for small angle x-ray scattering experiments. The spectroscopic features, correspond to electronic excited states in which an inner-shell electron has been excited to unfilled molecular orbitals or conduction bands. They are determined by the bonding environment and thus provide a characteristic signature for every material.

The selective enhancement or suppression of the scattering in connection with chemical differences was demonstrated for the carbon C K-edge by using latex spheres of two different chemical compositions (polystyrene and polymethyl methacrylate; PS and PMMA respectively). These lattices were also of different sizes (80nm for PS and 300 nm for the PMMA). In figure 1 we have plotted the scattering intensity (the square of the scattering factor) for the PS and PMMA, calculated from the absorption spectra, using the relationships in equations 1-3.

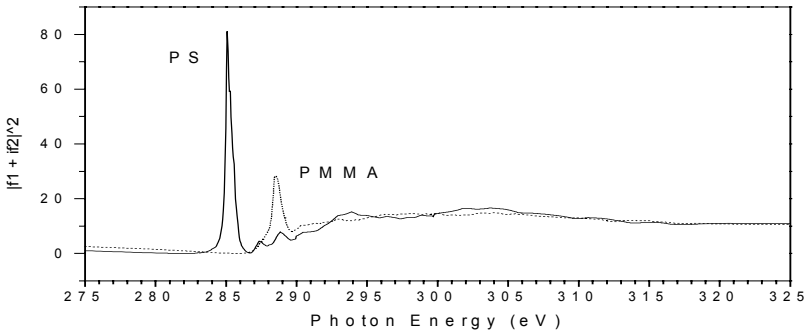

Figure 1. Scattering intensity (f^2) of PMMA and PS calculated from the measured NEXAFS spectra.

RESULTS AND DISCUSSION

NEAXFS spectra were measured from thin films of the lattices dispersed onto thin (100nm) Si_3N_4 windows using the BL7.0.1 scanning transmission x-ray microscope. The most intense peak for both materials is the C1s --> π^* transition which is associated with C=C bonds in PS and C=O bonds in PMMA. Fortuitously, the weakest scattering for each material occurs at energies just below the maximum intensity peak. In Figure 2 the scattering intensity as a function of scattering vector ($q = (4\pi/\lambda)\sin\theta$; θ = scattering angle) is plotted for PS and PMMA samples at the energies for minimum and maximum scattering intensities in each case. The patterns indeed show strong oscillations when measured at the peak scattering intensity and are relatively featureless at the energy of the minimum. In agreement with the relative sizes of the latex particles, one observes that the features in the scattering pattern for PMMA begin at lower q than those for the PS latex. The data can be analyzed by fitting to calculated scattering curves (not shown) and when this is done one retrieves information on particle size consistent with the data provided by the manufacturer measured by other methods. It is interesting to note that deviation of the experimentally acquired data from the calculated pattern occurs and can likely be attributed to the important interfacial or superficial structure of the lattices. This aspect of the data analysis is still under scrutiny by us.

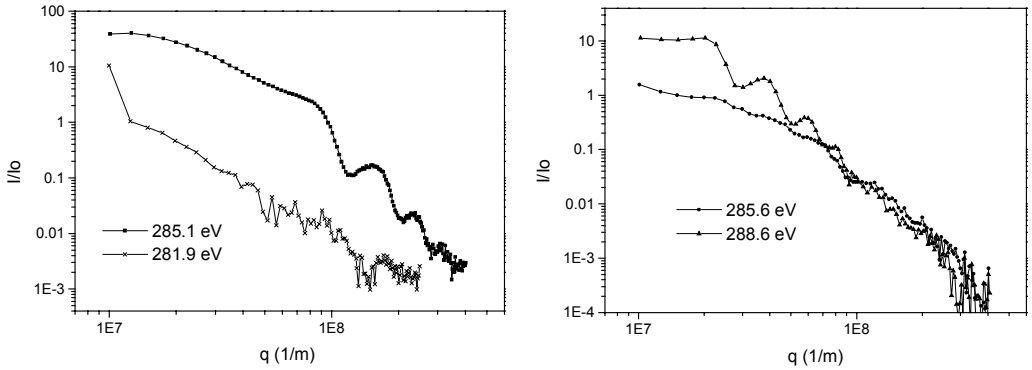

Figure 2. Scattering patterns measured as a function of q for PMMA latex spheres nominally 80 nm in diameter (right) and PS latex spheres nominally 300 nm in diameter (right).

In another experiment, samples of both of the two lattices were randomly dispersed (dried) onto the same Si_3N_4 window. This experiment demonstrates one powerful aspect of this polymer characterization method. When the scattering pattern is measured at 260 eV, well away from any absorption resonances, it appears to be a sum of scattering from both phases. However, at 281.9 eV the scattering from the PS spheres is suppressed and the pattern is dominated by features due to the PMMA spheres. On the other hand, when the data is measured with a photon energy of 285.6 eV the PMMA scattering is suppressed and the pattern is dominated by scattering from PS spheres. Figure 3 shows that in order to determine the structure of one material in the presence of the other, one may acquire the scattering patterns at the energies at which scattering from one phase and then the other phase is enhanced.

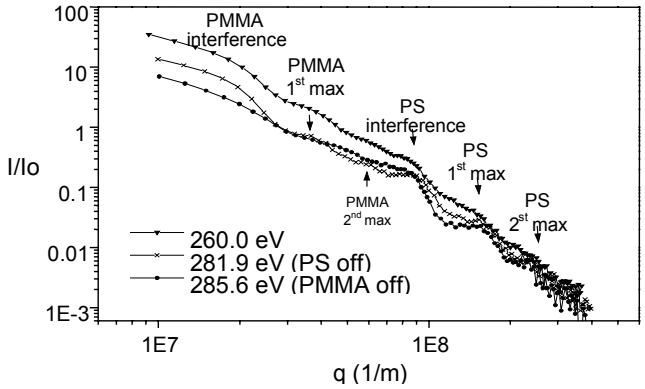

Figure 3. Scattering patterns measured as a function of q for a mixture of the PS latex spheres, nominally 80 nm in diameter and PMMA latex spheres, nominally 300 nm in diameter acquired at the indicated photon energies.

SUMMARY

The presented experiment combines the power of small-angle scattering for sub microscopic structural information with the carbon near-edge absorption fine structure as contrast mechanism for chemical composition. This approach is believed to be useful in several areas where multiphase material are being studied, including polymer blends, structured lattices, soft organic based colloidal materials, advanced electronic materials, structured compound materials, multiphase systems, and nanocomposites.

REFERENCES

1. A. Guinier, Ann. phys. 12, 161 (1939).
2. H. B. Stuhrmann, "Resonance Scattering in Macromolecular Structure Research", in "Advances in Polymer Science" vol. 67 edited by H. Kausch and H. Zachmann, 123-163 Springer-Verlag, Berlin (1985).
3. J. B. Kortright and Sang-Kong Kim, Physical Review B, 62 (2000) 12 216.
4. D. Atwood, "Soft X-Rays and Extreme Ultraviolet Radiation Principles and Applications", Cambrideg University Press, (1999)90-94.
5. H. Ade and S. G. Urquhart, "NEXAFS Spectroscopy and Microscopy of Natural and Synthetic Polymers", In *Chemical Applications of Synchrotron Radiation*, T. K. Sham, Ed. (World Scientific Publishing, Singapore, to be published.
6. J. Stöhr, *NEXAFS Spectroscopy*, Springer-Verlag, Berlin, 1992.

This work was supported by The Dow Chemical Company. One of us (JK) was supported by the Director, Office of Science, Office of Basic Energy Sciences of the U. S. Department of Energy under Contract No. DE-AC0376SF00098.

Contact: Gary Mitchell, Dow Chemical, V: 989 636-3666, email: gemitchell@dow.com

Soft X-Ray Emission and Absorption Spectra in the Si *L* Region of Polysilanes

Y. Muramatsu[1], M. Fujino[2], E. M. Gullikson[3] and R. C. C. Perera[3]
[1]*Japan Atomic Energy Research Institute, Sayo-gun, Hyogo 679-5148, Japan*
[2]*NTT Basic Research Laboratories, Atsugi, Kanagawa 243-0198, Japan*
[3]*CXRO, Lawrence Berkeley National Laboratory, Berkeley, California 94720, USA*

Substituted polysilanes, (SiRR')n, have attracted significant attention because of their unique electronic properties. Their characteristic electronic nature arises from band edge structures which are composed of valence and conduction bands from σ and σ* bands, respectively, which differ from the electronic structure of polyacetylene. To further understand their electronic properties, we have measured the Si *L* x-ray emission spectra of a number of polysilanes with alkyl and phenyl substituents. In addition, their x-ray absorption spectra have also been measured to obtain information regarding unoccupied electronic orbitals.

Chemically synthesized polysilanes, $(SiR_2)n$, where R indicates substitution with a methyl (Me; CH_3), ethyl (Et; C_2H_5), propyl (Pr; n-C_3H_7), butyl (Bu; n-C_4H_9), pentyl (Pe; n-C_5H_{11}) or phenyl (Ph; C_6H_5) group, were used for spectroscopic measurements. Soft x-ray emission spectra in the Si *L* region were measured using a grating x-ray spectrometer installed in the undulator beamline, BL-8.0.1. The photon energy of the monochromatized incident beam was tuned to about 130 eV to effectively excite Si2p-electrons while preventing multiple ionizations. Total-electron-yield (TEY) x-ray absorption spectra were obtained by monitoring sample photocurrent in BL-6.3.2. Measured x-ray emission and absorption spectra were analyzed using discrete variational (DV)-Xα molecular orbital calculations.

Figure 1 shows soft x-ray emission and absorption spectra in the Si *L* region of both the polysilanes and the reference compounds, Si and SiO_2. In the emission spectra, polysilane spectral features exhibited similar structures; a main peak near 90 eV, and high-energy and low-energy shoulders clearly differ from those of the Si and SiO_2 references. In absorption spectra, alkyl-substituted polysilanes exhibit a threshold energy of 101 eV, while the Ph-substituted polysilane exhibits a slightly lower threshold energy. In the fine-structure at the thresholds of polysilanes, a pre-edge peak is observed near 101 eV and an intense peak is seen at 102 eV for the Ph-substituted polysilane. No such pre-edge or intense peaks, however, are observed in the spectra of alkyl-substituted samples. From spectral analysis using DV-Xα molecular orbital calculations Si *L* x-ray emission spectra, which include a main peak with high- and low-energy shoulders, are explained by the summed DOS spectra of occupied Si3s and Si3d orbitals hybridized with Si3p, C2s and C2p orbitals. X-ray absorption spectra are also qualitatively explained by the summed DOS spectra of unoccupied Si3s and Si3d orbitals. In both x-ray emission and absorption spectra, little difference is observed among alkyl-substituted polysilanes. It is therefore confirmed that the length of alkyl substituents has little effect on the electronic structure of the Si backbone. X-ray spectral features of the Ph-substituted polysilane, however, slightly differ from alkyl-substituted features. This is explained by the difference in hybridization of Si and C orbitals between sp^2-C atoms in phenyl substituents and sp^3-C atoms in alkyl ones.

We thank Dr. J. Denlinger of the Lawrence Berkeley National Laboratory for his help and support in performing x-ray emission measurements. This work has been supported by the Hyogo Science and Technology Association and the US Department of Energy under contract No. DE-AC03-76SF00098.

Principal Investigator: Yasuji Muramatsu, Japan Atomic Energy Research Institute. Email: murama@spring8.or.jp. Telephone: +81-791-58-2601.

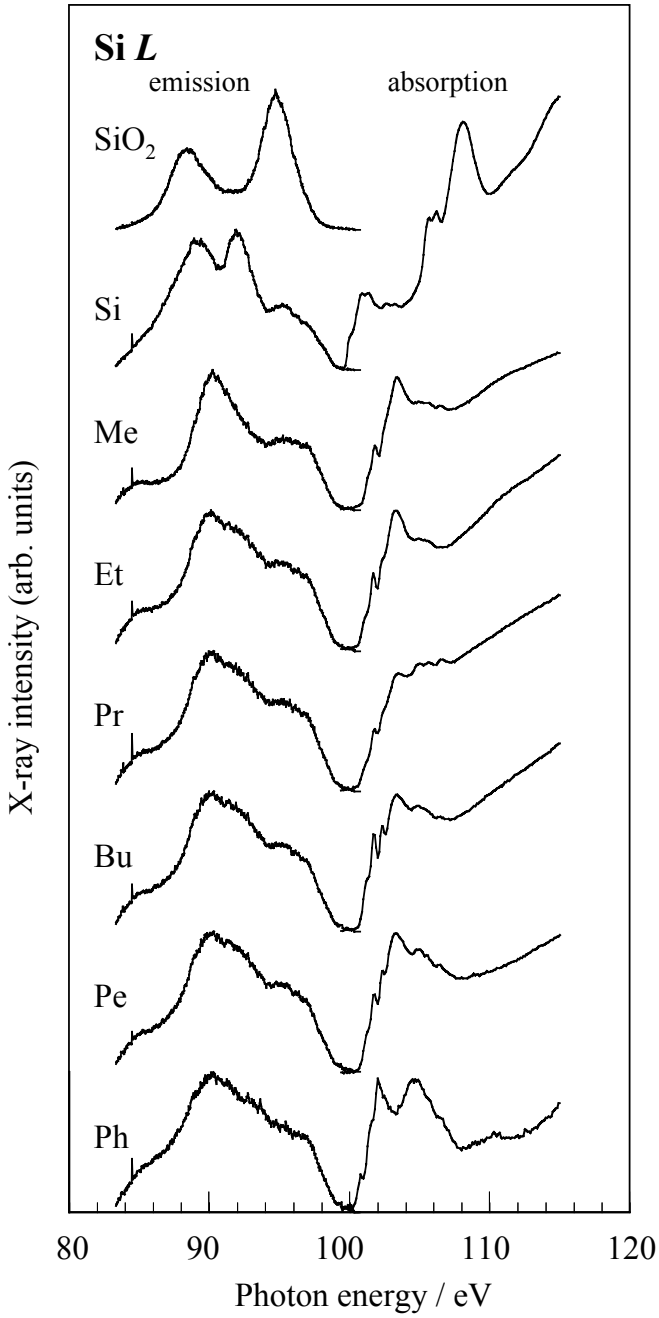

Figure 1 Soft x-ray emission and TEY x-ray absorption spectra in the Si *L* region of the polysilanes, $(SiR_2)n$, and Si and SiO_2 reference compounds. Substituents in the polysilanes, R, are denoted by Me (CH_3), Et (C_2H_5), Pr (n-C_3H_7), Bu (n-C_4H_9), Pe (n-C_5H_{11}), and Ph (C_6H_5).

Soft X-Ray Spectroscopy of Noble Gas Atoms Doped in Solid Matrices

Y. Muramatsu[1], and R. C. C. Perera[2]

[1]*Japan Atomic Energy Research Institute, Sayo-gun, Hyogo 679-5148, Japan*

[2]*CXRO, Lawrence Berkeley National Laboratory, Berkeley, California 94720, USA*

We have measured the soft x-ray emission and absorption spectra of noble-gas atoms doped in carbon, silicon and metal substrates, to investigate their chemical states in solid matrices. Argon or neon ion beams were directed into the solid matrices of highly oriented pyrolytic graphite (HOPG), Si(111), SiO_2, Ti, Cr, Ni and Cu with an acceleration voltage of 5 kV. Soft x-ray emission and absorption spectra in the Ar *L* and Ne *K* regions of Ar- and Ne-doped samples were measured using a grating x-ray spectrometer installed in the undulator beamline, BL-8.0.1. Figure 1 shows the Ar *L* x-ray emission spectra of Ar-doped Si(111) measured with excitation energies of (a) 399.6 eV and (b) 256.6 eV. The subtracted spectrum of (a) – (b), clearly indicates that peak structures are observed on the higher-energy sides of both $L\alpha$ and $L\beta$ peaks arising from 399.6-eV excitation. These peak structures may be due to multiple ionizations. Figure 2 shows the Ar *L* x-ray emission spectra of Ar-doped Si(111), HOPG, Ti and Cu measured with 256.6-eV excitation. Peak widths of $L\alpha$ and $L\beta$ peaks in the Ar *L* x-ray emission spectra from Ti and Cu matrices are broader than that of the Si(111) and HOPG matrices. A similar peak broadness was also observed in the Ne *K* x-ray emission spectra of Ne-doped metal matrices. Such peak broadness may be explained by the formation of noble gas bubbles in the metals. To further explain peak broadness in the spectra, molecular orbital calculations are currently in progress. We thank Dr. J. Denlinger of the Lawrence Berkeley National Laboratory for his help and support in performing x-ray emission measurements. This work has been supported by the Hyogo Science and Technology Association and the US Department of Energy under contract No. DE-AC03-76SF00098. Principal Investigator: Yasuji Muramatsu, Japan Atomic Energy Research Institute. Email: murama@spring8.or.jp. Telephone: +81-791-58-2601.

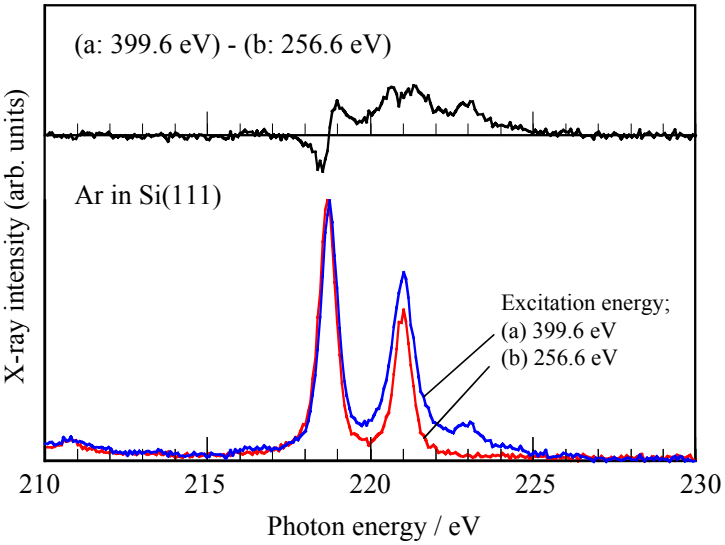

Figure 1 Ar *L* x-ray emission spectra of Ar-doped Si(111) with excitation energies of (a) 399.6 eV and (b) 256.6 eV. Upper panel shows the subtracted spectrum, (a) – (b).

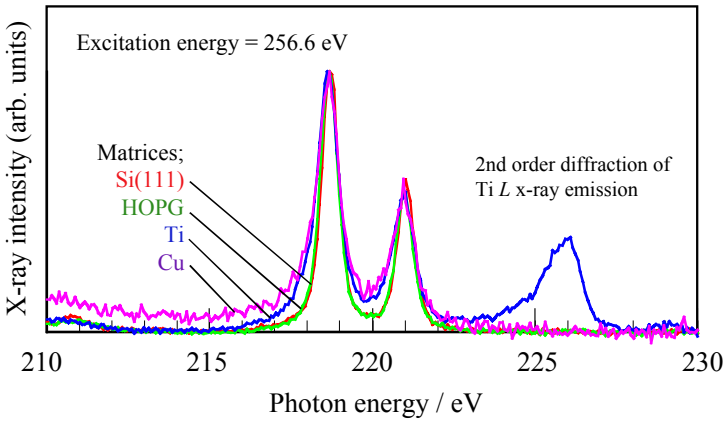

Figure 2 Ar *L* x-ray emission spectra of Ar-doped Si(111), HOPG, Ti, and Cu matrices. Excitation energy was tuned to 256.6 eV.

X-RAY ABSORPTION STUDIES OF THE cBN COMPOSITES WITH DIFFERENT BONDING PHASES

E. Benko[a], K. Lawniczak-Jablonska[b], P. Nachimuthu[c], I. N. Demchenko[b], E. Piskorska[b], P. Klimczyk[a], R.C.C Perera[c], A. Włochowicz[d], A. Benko[e], T. L. Barr[e]

[a]*Institute of Metal Cutting, Wroclawska 37A Str., 30-011 Cracow, Poland*
[b]*Institute of Physics Polish Academy of Science, Al. Lotnikow 32/46, 02-668 Warsaw, Poland*
[c]*Center for X-ray Optics, Lawrence Berkeley National Laboratory, University of California –Berkeley, Berkeley, California 94720*
[d]*University of Bielsko Biała , Willowa 2 Str., 43-309 Bielsko-Biała*
[e]*Materials Department and Laboratory for Surface Studies, University of Wisconsin-Milwaukee, Milwaukee, WI 53201, USA*

The cBN composites are widely used in various applications because of their excellent wear and corrosion resistance and their thermal and electronic properties. In order to obtain composition materials with optimal properties and using economic and safe for environment technology it is important to recognize chemical reactions occurring at boron nitride during formation of bonding phase. Titanium and their compounds are most commonly used as binders in sintering technology. We present the results of studies of cBN composites with addition of TiN and TiC ceramics to form a bonding phase. The wider class of additions is under investigation.

From thermodynamical calculations it follows that in the temperature range from 1000 to 1400^0C TiC and TiN react with cBN forming in the case of TiC two new phases (TiB_2 and $TiC_{0.8}N_{0.2}$) and only TiB_2 phase in the case TiN addition.

Composites were prepared by high pressure (9GPa) hot pressing (1750^oC) and the samples were subsequently heat treated at 1000 and 1400^oC for 1 hour in vacuum $3*10^{-3}$ Pa. Sinters of cBN-TiN/TiC before and after heat treatment were characterised using transmission electron microscopy and X-ray absorption technique.

RESULTS AND DISCUSSION

TEM studies of the microstructure in cBN sintered with TiN and heated up to 1400 ^{o}C

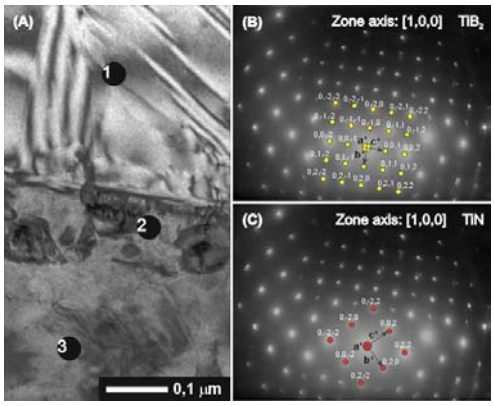

The microstructure of cBN sintered with TiN is compact. Analysis of the electron diffraction (Fig.1, B and C) allowed to conclude that the fine crystallites at the boundary show the TiB_2 phase (B) whereas the bigger grains inside the TiN phase (C). The cBN/TiC compact looks the same like cBN/TiN. But in some places the electron diffraction pattern indicates on the presence of the triple Ti(BC) compound.

Fig.1. Boundary between the two fine-crystalline area of cBN/TiN composite (A) and electron diffraction pattern from the point 2 (B) and 3 (C).

X-ray absorption study

X-ray absorption measurements were carried out at the Advanced Light Source of Lawrence Berkeley National Laboratory (beamline 6.3.2) and at the HASYLAB in Hamburg. (beamline A1). As an example are presented XANES at the Ti K-edge of cBN/TiN (Fig.2) and

Ti $L_{2,3}$-edge (Fig.3) from cBN - TiC/TiN.

Spectra show formation of the TiB_2 new phase after heating to 1300^0C, without heat treatment TiB_2 was not formed (Fig.2). The formed TiB_2 phase is not ideal, it can have defects and inclusions of other phases. The possibility of the foreign phases addition was check (upper curves) and conclusion can be drown that addition to the TiB_2 phase up to 30% of TiN phase does not improve the agreement between modelled and observed phase. In composites without heat treatment the inclusions of up to 20% TiC and 10% TiB_2 cannot be excluded.

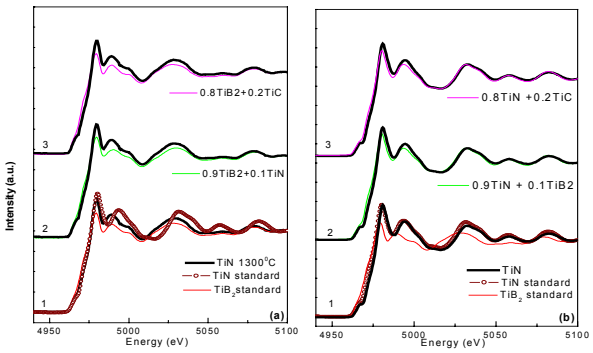

Fig. 2. The Ti K - edges of the cBN/TiN and reference samples heated up to 1300^0C (a) and cBN/TiN without heat treatment (b).

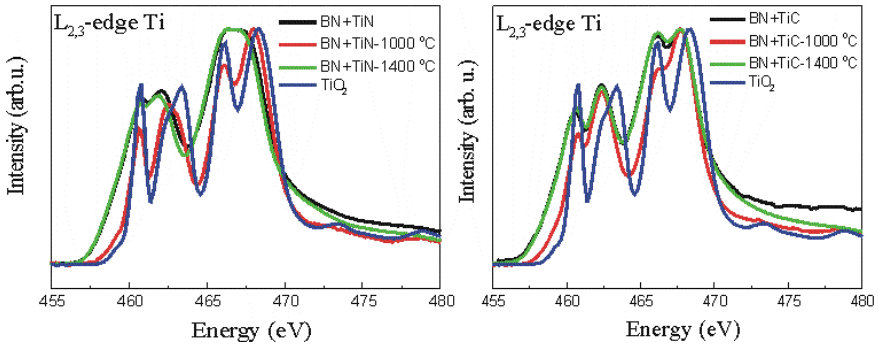

Fig.3. Ti $L_{2,3}$ x-ray absorption edge spectra of cBN/TiN and cBN/TiC composites before and after heat treatment and TiO_2 as reference.

The pick structure in Fig.3 shows formation of TiO_2 like phase in the cBN-TiN/TiC composites. It was proved that the temperature of 1000^0C was not high enough to avoid the oxidation of the composite grains, the heat treatment up to 1400^0C prevent the oxidation of grains.

Conclusion

X ray absorption measurements provide a clear spectroscopic signature of TiB_2 formation in the cBN-TiN/TiC composites. There was proved that the temperature of 1000^0C was not high enough to avoid the oxidation of the composite grains, therefore the heat treatment is necessary. The formed TiB_2 phase is not free from the defects but we do not observed foreign phase inclusion after heating.
From the analysis of the edge shape one can conclude on the chemical processes and optimise of the BN-TiC/TiN composites heat treatment procedure.

Acknowledgements
This study is based on the work sponsored by Polish State Committee for Scientific Research (Grant No 7T08D 014 17) and SPUB (Grant No-M/DESY/P-03/ DZ-213/2000) and IHP-Contract HPRI-CT-1999-00040 of the European Commission.

Principal investigator: Krystyna Lawniczak-Jablonska, Institute of Physics, Polish Academy of Sciences. Telephone: 48 22 8436034. Email: jablo@ifpan.edu.pl.